

## Mobile Robot Enabled Detection of Explosives and Biological Agents

Gregory W. Auner<sup>1</sup>, Abhilash Pandya<sup>1</sup>, Golam Newaz<sup>1</sup>, Grant Gerhart<sup>2</sup>, Greg Hudas<sup>2</sup>, Andrew Scott<sup>2</sup>, Janet Jensen<sup>3</sup>, Joseph Smolinski<sup>1</sup>, and Michelle Brusatori<sup>1</sup>

<sup>1</sup>Wayne State University, SSIM Program, Detroit, Michigan 48202

<sup>2</sup>U.S. Army RDECOM-TARDEC, 6501 E. 11 Mile Rd., Warren, MI 48397-5000

<sup>3</sup>U.S. Army Edgewood CB Center, Aberdeen Proving Ground, MD 21010-5424

**Problem and Approach-** Detection of chemical agents such as explosives and biological agents in air and water is of current importance. The integration of micro sensors for agent detection into a robotic system can greatly enhance the safety and efficacy of the detection system. Our research aim is two-fold. 1) To create a sensing system that can detect chemical agents in explosives and biological agents in air and water and 2) to implement the detection technology into a handheld unit or a mobile robot system (such as ODIS-omni directional inspection system) that allows the soldier to deliver the sensing system to remote targets. In the case of explosives detection, the sensing system includes a thermoplastic polyurethane concentrator that absorbs the main vapor byproduct of TNT. This concentrator will release, in burst mode, higher levels of TNT vapor byproduct to allow detection under real environmental conditions. In addition, a biological sampling and concentration system can be implemented to detect small quantities of bacteria. Two methods of detection are implemented including a physical vapor detector and an optical probe detector. These lightweight miniature detection systems are integrated into a remote manipulator arm on the mobile robotic platform. The platform has an automatic scanning mode and motion control for flexible remote control.

**Explosives Detection-** Explosive charges are always accompanied by impurities such as 2,4-dinitro toluene (DNT), 2,6-DNT, 1,3-dinitro benzene (DNB) and 2,4-DNB in the TNT, and these impurities generate higher vapor concentrations than 2,4,6-TNT itself.<sup>1</sup> 2,4-DNT is an impurity, as a solid constituent in the range of  $9.32 \times 10^{-5}$  to  $7.43 \times 10^{-4}$  g/g of TNT at 22 °C in the military grade TNT. A headspace vapor constituent of 2,4-DNT was  $6.9 \times 10^{-11}$  to  $1.9 \times 10^{-9}$  g/g, which is significantly higher than 2,4,6-TNT. Similarly, 1,3-DNB is another impurity in the range of  $1.39 \times 10^{-5}$  to  $8.88 \times 10^{-4}$  g/g of TNT at 22 °C. A headspace vapor constituent of 1,3-DNB was  $2.2 \times 10^{-11}$  to  $4.3 \times 10^{-9}$  g/g. This is due to the fact that the vapor pressure of 2,4-DNT and 1,3 DNB are approximately 40–1000 times greater than the vapor pressure of TNT. Our detection system will detect 2,4-DNT and 2,3-DNB vapors as signature of TNT-based explosives. The sensing system or explosive vapor detection module is composed of 4 technological components (Figure 1). The development of a pre-concentrator fabricated into a honeycomb structure with integrated a low power micro heater. This polymer specifically absorbs DNT and DNB vapor. In addition,

concentrators coated with carbowax have also been tested. The pre-concentrators high absorption levels for DNT and DNB chemical is reversed at a higher temperature. This material can be used to absorb the background chemical signature and provide a concentrated burst for higher detection sensitivity. Vapor is pumped by an integrated MEMS micropump to one of two sensing systems.

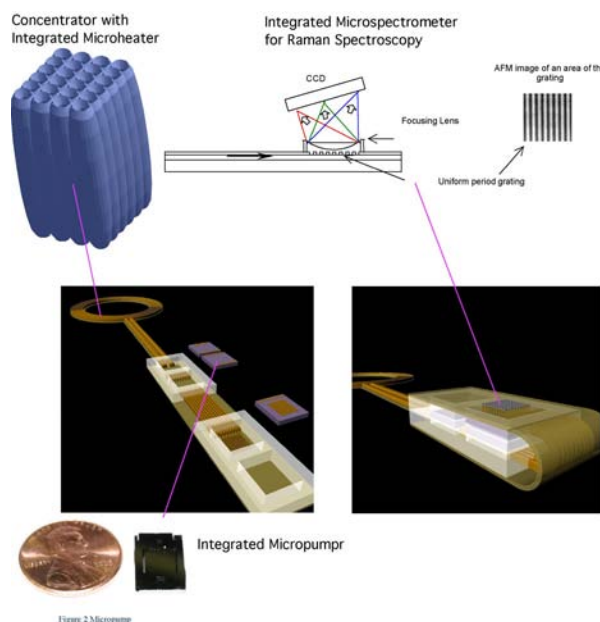


**Figure 1- Illustration of Raman microspectrometer with integrated microconcentrator.**

The first sensing method includes a micro channel based system terminated in a differential surface acoustic wave sensor.<sup>2,3</sup> Matching surface waves are compared with an acoustic wave device exposed to the sampling vapor and the other sealed. Explosive impurity concentrates are absorbed on the surface of the exposed surface acoustic wave sensor using a reactive carbowax polymer thin film (Figure 2). The combination of mass and polymer distortion creates a shift in acoustic wave frequency that is measured by a phase change detection system. This paper describes the use of an optical probe for (multispectral) Raman spectroscopy used to detect the chemical fingerprint of TNT components.

Spectra of highly diluted (parts per million) 2,4 DNT were obtained with both laser excitation lines and

| Report Documentation Page  |                                    |                                     | Form Approved<br>OMB No. 0704-0188         |   |                                    |
|--|------------------------------------|-------------------------------------|--|---|------------------------------------|
| Public reporting burden for the collection of information is estimated to average 1 hour per response, including the time for reviewing instructions, searching existing data sources, gathering and maintaining the data needed, and completing and reviewing the collection of information. Send comments regarding this burden estimate or any other aspect of this collection of information, including suggestions for reducing this burden, to Washington Headquarters Services, Directorate for Information Operations and Reports, 1215 Jefferson Davis Highway, Suite 1204, Arlington VA 22202-4302. Respondents should be aware that notwithstanding any other provision of law, no person shall be subject to a penalty for failing to comply with a collection of information if it does not display a currently valid OMB control number. |                                    |                                     |  |   |                                    |
| 1. REPORT DATE<br><b>01 NOV 2006</b>   |                                    | 2. REPORT TYPE<br><b>N/A</b>        |  | 3. DATES COVERED<br><b>-</b>                |                                    |
| 4. TITLE AND SUBTITLE<br><b>Mobile Robot Enabled Detection of Explosives and Biological Agents</b>   |                                    |                                     |  | 5a. CONTRACT NUMBER                         |                                    |
|  |                                    |                                     |  | 5b. GRANT NUMBER                            |                                    |
|  |                                    |                                     |  | 5c. PROGRAM ELEMENT NUMBER                  |                                    |
| 6. AUTHOR(S)   |                                    |                                     |  | 5d. PROJECT NUMBER                          |                                    |
|  |                                    |                                     |  | 5e. TASK NUMBER                             |                                    |
|  |                                    |                                     |  | 5f. WORK UNIT NUMBER                        |                                    |
| 7. PERFORMING ORGANIZATION NAME(S) AND ADDRESS(ES)<br><b>Wayne State University, SSIM Program, Detroit, Michigan 48202</b>   |                                    |                                     |  | 8. PERFORMING ORGANIZATION<br>REPORT NUMBER |                                    |
| 9. SPONSORING/MONITORING AGENCY NAME(S) AND ADDRESS(ES)  |                                    |                                     |  | 10. SPONSOR/MONITOR'S ACRONYM(S)            |                                    |
|  |                                    |                                     |  | 11. SPONSOR/MONITOR'S REPORT<br>NUMBER(S)   |                                    |
| 12. DISTRIBUTION/AVAILABILITY STATEMENT<br><b>Approved for public release, distribution unlimited</b>  |                                    |                                     |  |   |                                    |
| 13. SUPPLEMENTARY NOTES<br><b>See also ADM002075., The original document contains color images.</b>  |                                    |                                     |  |   |                                    |
| 14. ABSTRACT   |                                    |                                     |  |   |                                    |
| 15. SUBJECT TERMS  |                                    |                                     |  |   |                                    |
| 16. SECURITY CLASSIFICATION OF:  |                                    |                                     | 17. LIMITATION OF<br>ABSTRACT<br><b>UU</b> | 18. NUMBER<br>OF PAGES<br><b>7</b>          | 19a. NAME OF<br>RESPONSIBLE PERSON |
| a. REPORT<br><b>unclassified</b>   | b. ABSTRACT<br><b>unclassified</b> | c. THIS PAGE<br><b>unclassified</b> |  |   |                                    |

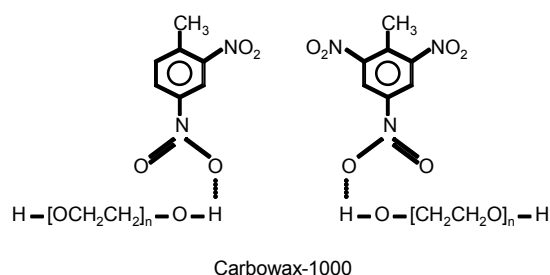


**Figure 2- Carbowax chemistry for binding DNT molecules for detection by acoustic wave or for trapping for photonic detection.**

are shown in Figure 3. The spectra are very intensive and easily obtainable with either excitation line, but the Raman scattering is typically one order of magnitude stronger when the 785nm excitation line is used.

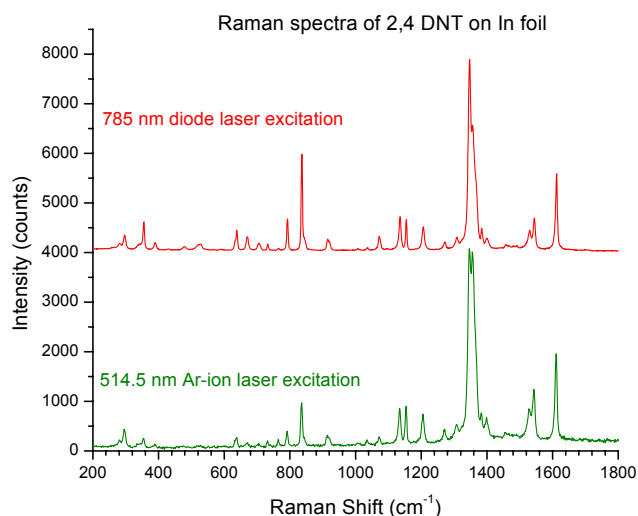


**Figure 3- Raman spectra at two wavelengths identifying TNT constituents.**

For final sample verification we investigated direct sampling of explosive phantoms with trace TNT. The Raman spectra were taken from the circular island on a substrate and from the TNT-solution-treated region on the PU sample. Both the 514.5nm and the 785nm laser excitation lines of our micro-Raman spectrometer were utilized. The results are shown the Figures 4 (green excitation) and Figure 5 (NIR excitation). The results indicate that explosives can be detected by both trapped DNT vapor and direct TNT sampling using Raman spectrometry. We have developed a micro spectrometer on a chip for integration into a robotic platform that is specifically designed for high sensitivity and high resolution of in the spectral region of interest.<sup>4-7</sup>

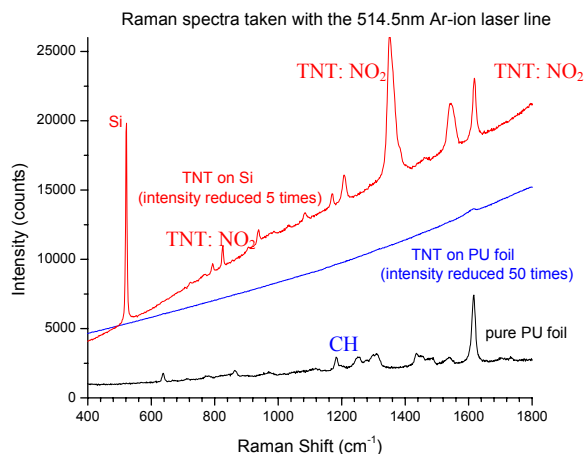


**Figure 4- Raman spectra using 514.5 green excitation wavelength directly on TNT sample.**

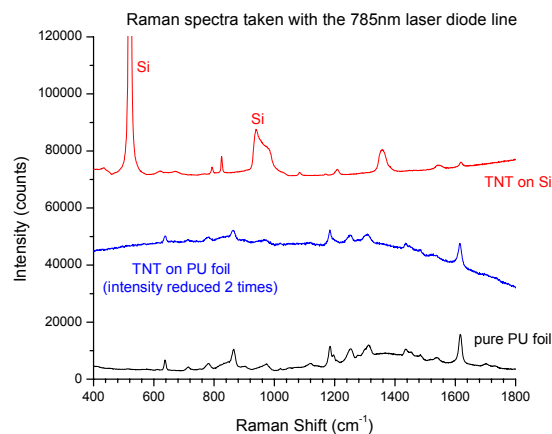


**Figure 5- Raman spectra using 785 nm NIR excitation wavelength for direct TNT detection.**

### Biological detection

Figure 6 below illustrates the system configuration for biological detection in water and air. Water to be sampled is pumped into a pre-sampling chamber where an ultrasound (US) device disperses pathogen colonies into individual bacteria. For air monitoring, samples are perfused into a liquid media. A primary filter (filter<sub>1</sub>) selectively allows bacteria at a predetermined size range to pass through to the detection system. This bacterial population is then infused into a concentrator chamber by using filter<sub>2</sub> with pore size that allows only water to go through. After sampling a large volume of water, a second pump directs a small volume of water with concentrated bacteria to the sensor. Here two types of sensors are utilized. The first is a dual mode acoustic wave device that can be used in a surface acoustic wave

mode for air samples or switched to a surface horizontal mode for liquids.<sup>8</sup>

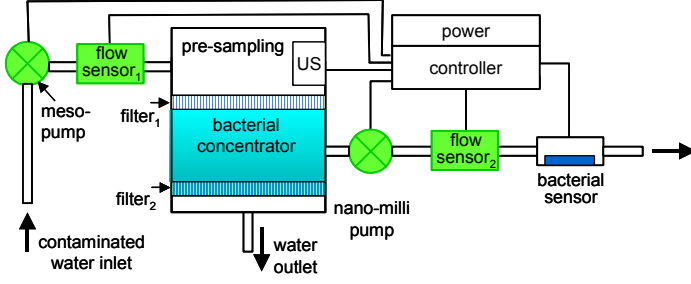


**Figure 6-Water Quality Sensing System.**

The acoustic wave device creates a primary surface mode and a secondary horizontal mode for detection. In order to determine the nature of the 2<sup>nd</sup> modes, we investigated their damping behavior by studying their transmission response under fluidic loading of the film. In Figure 7, we show the frequency response of such a device before and after a 3  $\mu$ l fluid loading. The ungated frequency response is displayed here for better observation of the insertion loss. One observes that the damping effect in the higher velocity mode is quite small,  $\sim 4$  dB, in contrast to 30 dB for the SAW mode. This suggests that the 2<sup>nd</sup> mode is likely a SH-SAW that couples weakly to the loaded fluid and is thus able to propagate without much attenuation. We have immobilized spherical phage receptor proteins for selective binding or capture of bacteria. The captured bacteria create a phase shift due to mass loading and other perturbation effects. In order to develop a compact detection system for integration into a mobile robot we developed a new highly sensitive RF circuit design.

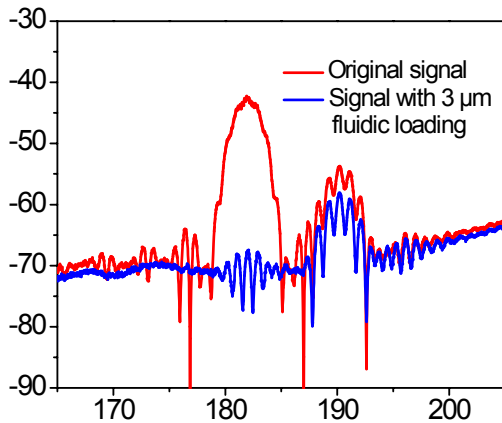


**Figure 7 - Damping of the SAW and SH mode under liquid loading at wavelength  $\lambda=32 \mu\text{m}$ .**

One of the major challenges is the physical design of a RF circuitry that can provide continuous and real time measurements capability, minimize parasitic and spurious noise, and obtain commensurable performance as bench top instruments while retaining a much smaller size. Without compromising the performance, the described RF circuitry should be small, inexpensive, and self-contained--including stable RF signal sources, easy sensor signal output capabilities, and excellent sensor input/output signal conditioning to suppress the noise floor, which dictates the detection limit.

There are basically two existing approaches for sensor signal read-out: one by monitoring the phase change of the sensors; the other by monitoring the frequency change of the sensors in oscillator feedback loops. The latter potentially can achieve higher detection resolution but has less tolerance to large signal magnitude fluctuation, which is common in liquid phase biosensing. For that reason we have focused on phase change based detection. The schematic diagram of the phase monitoring approach is shown in Figure 8. The amplitude and phase of two identical sensors are differentially compared with each other. The signal source is a voltage controlled oscillator, which supplies a pure sinusoidal wave for two sensors via a power splitter. The differential sensor pairs are wire bonded onto a ceramic hybrid chip. The input/output signal conditioning part is composed of transformers and sensor

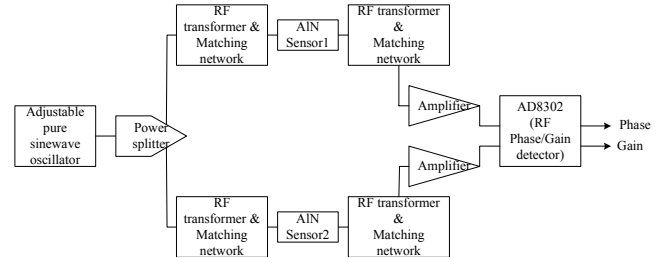


**Figure 8- Schematic of the phase monitoring circuit.**

impedance matching network to achieve a low noise, high integrity signal response. The two primary outputs from the system are voltages related to the amplitude ratio and phase difference that are caused by the sensor's response to analyte sorption by the coated immobilization layer:

$$V_{\text{mag}} = k \log(V_{s1} / V_{s2})$$

$$V_{\text{phs}} = k_{\phi} [\Phi_{s1} - \Phi_{s2}],$$

where  $V_{\text{mag}}$  is one output voltage that is proportional to the amplitude ratio  $V_{s1}/V_{s2}$  of the two sensors and  $V_{\text{phs}}$  is the other output voltage that is proportional to the phase difference,  $\Phi_{s1} - \Phi_{s2}$ , of the two sensors. The simple voltage output of the system eliminates the needs for sophisticated data acquisition interface.

The attributes such as size and cost effectiveness are especially important for the portable biosensor system. The prototype circuit is demonstrated in Figure 9, with dimensions of about 2 x 4 inch. The power supply for the circuit is designed to operate from a 9 VDC battery source to supply regulated +5 VDC and +12 VDC. The Analog Device's AD8302 is chosen as the key element for phase/amplitude measurements. This is a fully integrated system which enables an accurate measurement of either amplitude ratio over a  $\pm 30$  dB range scaled to 30 mV/dB, and of phase over a  $0^\circ$ – $180^\circ$  range scaled to 10 mV/degree. The initial test results show that the output voltage can be stabilized in 0.1 mV scale, which is equivalent to a phase resolution of less than 0.1 degree.

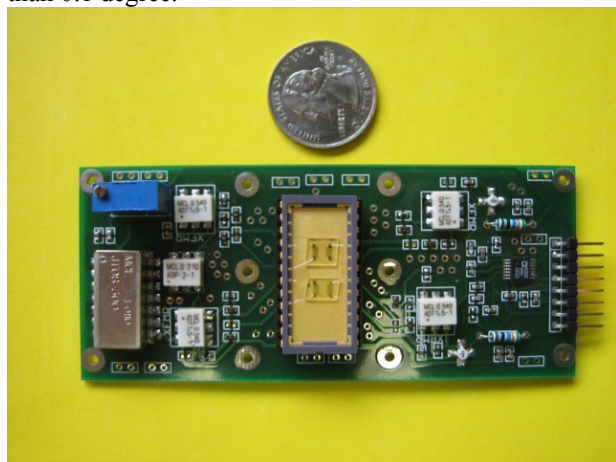


**Figure 9 - The circuit implementation monitoring phase/amplitude simultaneously.**

Figure 10 shows the result of mass loading of the device. Here, phase change shifts are indicated with loading of the active surface of the exposed sensor. The relative shift indicates a strong signal change and sensitive detection with less than 1% binding on the surface. In addition, relative quantities of bacteria can be derived from the signal.

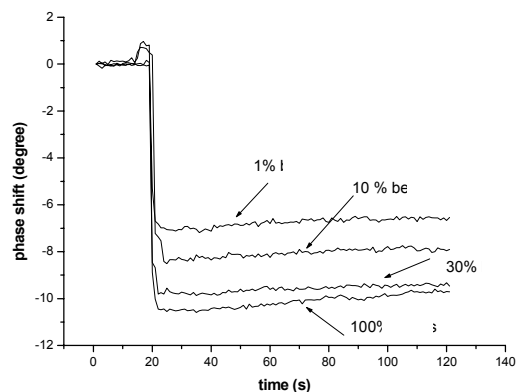


**Figure 10- Phase change due to mass loading on the acoustic wave sensor.**

## Detection by micro Raman Spectrometry

Sensing by a “chemical sniffing canine” is based on a combination of the chemical binding of molecules in the nose and the vibration of that particular molecule. The combination of these two sensing methods provides a very sensitive and selective detection method. As in the case of explosive detection, Raman spectroscopy uses laser reflection signals to detect the signature vibrations of molecular and chemical structures. Large sophisticated Raman instruments have been used to detect a number of toxins, chemicals and recently

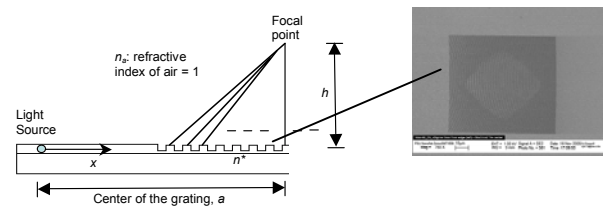


**Figure 11- Illustration of micro spectrometer for Raman system with photo of the fabricated 2-dimensional self-focusing grating.**

biological agents. The solution is a miniaturized version of the Raman spectrometer for a Chemical and Biological Sniffer (CBS) as shown in Figure 11

We have analyzed and developed libraries of Raman signatures for a number of biological and chemical agents. This information is used to develop a micro Raman system that consists of a number of concurrent detecting micro spectrometers, each of which is only a few millimeters in size. With this new technology, the known selective spectroscopic peaks that signify a particular bacteria or chemical agent can be registered in parallel. The micro spectrometers can be optimized for ultra low noise and high sensitivity for each of these identified peaks. This enables an extremely sensitive analysis that is faster, smaller and more powerful for detection than the current tabletop system. This system could be packaged in an ultra small hand held unit that is mass producible and can withstand adverse environments without the need for reagents.

We are currently cataloging a variety of waterborne bacteria strains in order to determine which regions and peaks can be used to uniquely identify the targeted bacterial species. The averaged runs of *E. coli* K99 in DI, *Strep Agalactiae*, *Salmonella*, *E. coli* K12 and DI water are shown in Figure 11. The results indicate a high degree of repeatability. Some peaks in the range 1200-1600 and the range 2800-3050 may be indicative to showing the presence of bacteria. The peaks found at 1335 1/cm and 1442 1/cm have been identified in the literature as CH and CHI deformations respectively. The triplet of peaks located in the region 2800-3200 1/cm have been described in literature as indicators of the

presence of bacteria and the results offer the possibility of being used as a general marker to determine the presence of biological agents.

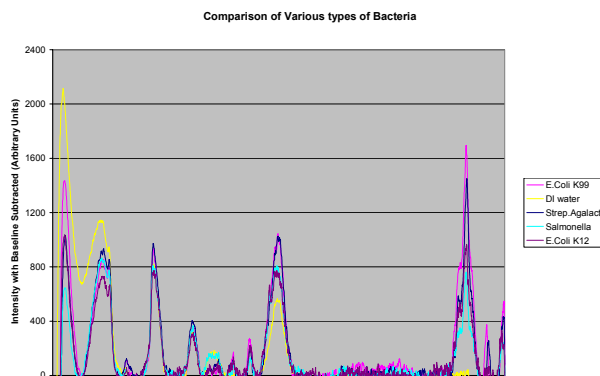


**Figure 11- Raman spectra comparison for DI water, *E. coli* K99, *E. coli* K12, Strep Agalactiae, Salmonella, and DI water.**

We are continuing to look for peaks that will distinguish bacteria strains from one another such as the Raman shift seen in Figure 12 in a comparison of Strep Agalactiae, gram positive bacteria, and *E. coli* 99, gram negative bacteria. Statistical analysis of approximated 10-20 runs for *E. coli* and Strep Agalactiae indicate this shift is real.

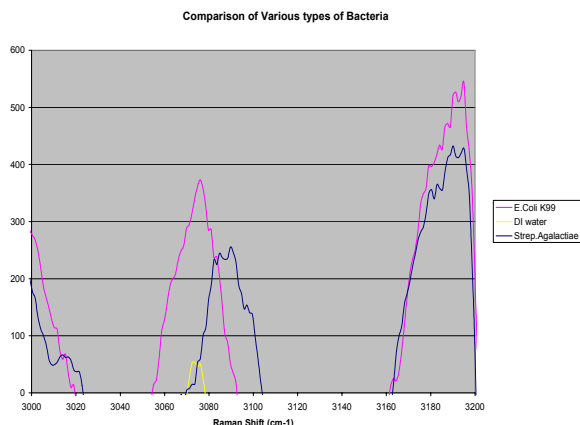


**Figure 12 – Raman shift in region 3050-3100 1/cm may be a point to identify the difference between *E. coli* K99 and Strep Agalactiae.**

In addition, preliminary results have confirmed our ability to detect unique signatures for bacterial endotoxins for *E. coli* and Salmonella as shown in Figure 13. The results may indicate an important distinguishing pattern using Raman biomarkers for LPS toxin. One strategy is to use the endo or exotoxin biomarker as a

distinguishing feature for bacteria detection. This would allow the use of limited selective regions of analysis in the Raman spectroscopy signal. An optimized microspectrometer on a chip would be fabricated to specifically sense in these regions.

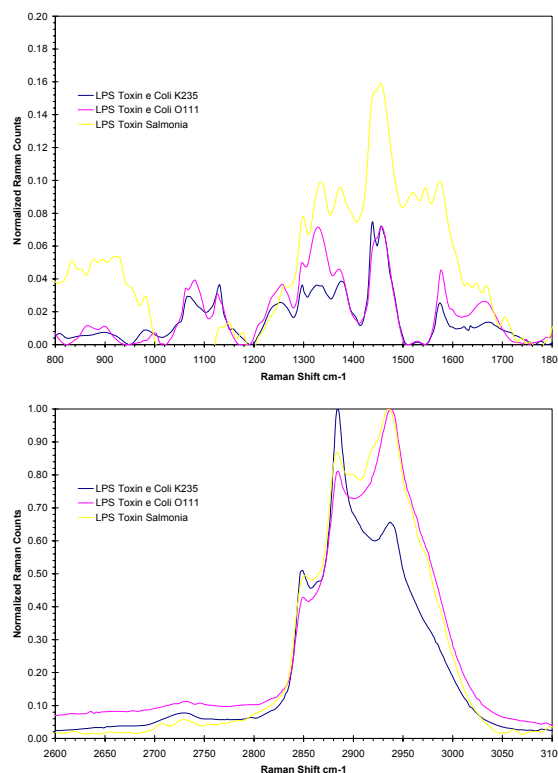


**Figure 13- The Raman spectrum of LPS toxins for *E.Coli* K235, *E. coli* O111, and Salmonella. The figure to the right is a localized region indicating LPS toxin.**

## Implementation

The sensing unit is an ultra compact MEMS (micro electro mechanical systems) system packaged with supporting electronics in an ultra lightweight sensing head. This allows direct integration into a robotic arm system for remote inspection. We have developed a wirelessly controlled 5 degree of freedom robotic arm that can be mounted to the Omni Directional Inspection system (ODIS; Figures 14 and 15)

We have developed the kinematics of the arm for ease of operation and perform soldier testing of the unit for a feedback in an iterative process of system design. We have also developed the human control interface teleoperation and semi autonomous commands required for a viable detection system. We are field-testing a prototype robotic system in the setting of a field exercise. This will provide validation of both of our technological capability and our detection models ensuring the best practices for rapid detection.

The ODIS platform is used as a mounting platform for various chemical and biological detection sensors.

Many sensors require close proximity to the object for detection purposes. As ODIS is a flat platform as shown in Fig 14, a robotic arm has been developed to provide dexterity for the mounted sensors. The sensors can be mounted on the arm that can be controlled remotely with the help of joysticks.



**Figure 14- ODIS robot**

The main criteria taken into consideration while designing the robotic arm was that it should be collapsible on the ODIS. The ODIS is required to perform under the car inspection, hence this criteria was critical in the design of the robot. The collapsible robot has five degrees of freedom and is equipped with a camera mounted on the end-effector.



**Figure 15- Left: Collapsible arm in extended position. Right: Collapsed position.**

Figure 15 shows the collapsible arm in the fully extended state and in the collapsible state. In the fully extended state, the arm stands 6 inches tall. Inverse kinematics algorithm was developed for the robot. This allowed the collapsible arm to be controlled with the help of two joysticks, one for rotation and one for translation. A graphical user interface and simulation was developed to understand the working envelope of the robot. Figures 16(a) and 16(b) shows the graphical user interface and its working envelope.

A camera mounted on the end-effector of the collapsible robot transmitted video signals over a wireless network. Two infrared sensors were mounted on

the ODIS platform to detect obstacles. A touch sensor was mounted on the end-effector of the collapsible arm.

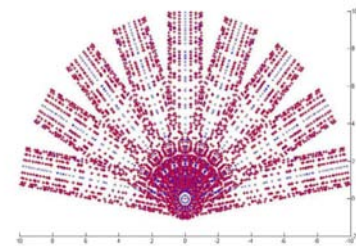
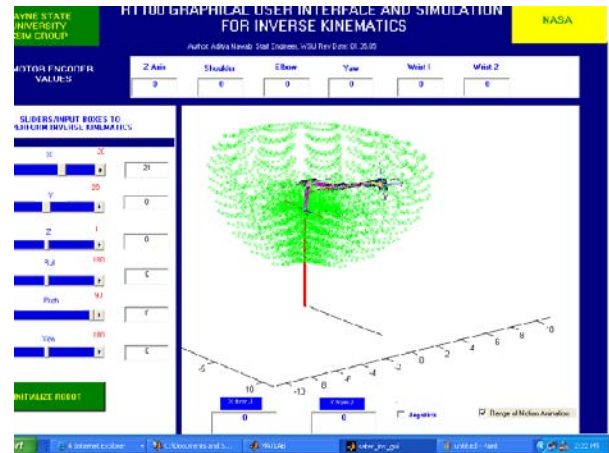


**Figure 16- (a) Graphical User interface for the arm and (b) its working envelope.**

The ODIS platform has a camera mounted in the front. Since proximity to the objects is a key factor for the sensors to give accurate results, human factors tests (Figure 17) were performed to determine which camera (end-effector or base) was better suited to navigate the robot by the tele-operator. The task was to approach the target within 2" of the target as quickly as possible. Ten subjects were used for a preliminary set of data. Time to task completion, distance from the target and the number of times the user bumped into the object were taken into consideration while evaluating the results. It proved that the end-effector camera was faster to navigate and there were less number of bumps than the base camera. This experiment helped us gain an insight whether or not to provide a camera as a payload on the end-effector and take that into consideration while calculating the load on the end-effector.

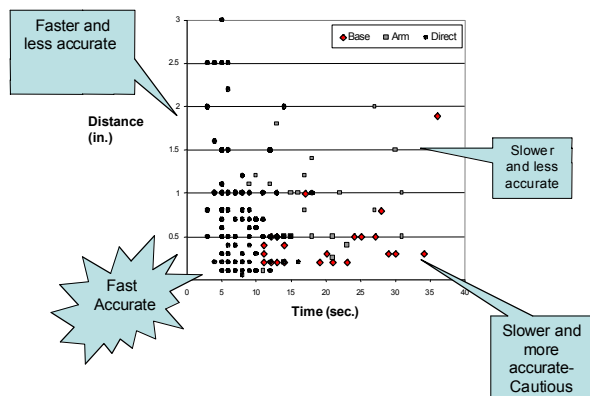


**Figure 17- Human factors testing using ODIS.**

**Relevance for Army-** For military applications, the Unmanned Ground Vehicle (UGV) System technology shown in this paper will greatly benefit the operators by reducing dangerous tasks to robotic operations through "stand-off". The detection of potential explosives/biological agents through advanced sensor system development along with the integration onto UGVs will provide benefits for applications of the Future Combat System (FCS) Small Unmanned Ground Vehicle (SUGV) system.

#### Acknowledgements

This work was supported by the Smart Sensors and Integrated Microsystems (SSIM) Program at Wayne State University, US Army contracts DAAE07-03-C-L140 and W56HZV-04-C-0044 and the National Institute of Health. Authors would also like to acknowledge the work of Dr. Jianzeng Xu and Qianghua Wang of Wayne State University, SSIM Laboratory.

#### References

- <sup>1</sup> G.K. Kannan, J.C. Kappor, Adsorption studies of carbowax and poly dimethyl siloxane to use as chemical array for nitro aromatic vapour sensing, *Sensors and Actuators B* 110 (2005) 312–320.
- <sup>2</sup> D.S. Ballantine, R. M. White, S. J. Marti, A. J. Ricco, E. T. Zeller, G. C. Frye, and H. Wohltjen, *Acoustic Wave Sensors: Theory, Design, and Physico-Chemical Applications*. San Diego: Academic Press, 1997.
- <sup>3</sup> G. Hu, H. Ying, X. Du, J. Xu, J. Smolinsky, and G. Auner, "Digital Phase Detection for High-Precision Surface Acoustic Wave Sensor Systems," *Proceedings of 2005 Joint IEEE International Frequency Control Symposium and Precise Time and Time Interval Systems*

*and Applications Meeting, Vancouver, BC, Canada, August 29-31, 2005.*

- <sup>4</sup> K. Chaganti, I. Salakhutdinov, I. Avrutsky, and G. Auner, "A simple miniature optical spectrometer with a planar waveguide grating coupler in combination with a plano-convex lens," *Optics Express*, vol. 14, pp. 4064-4072, 2006.
- <sup>5</sup> K. Chaganti, I. Salakhutdinov, I. Avrutsky, G. Auner, and J. Mansfield, "Sub-micron grating fabrication on hafnium oxide thin-film waveguides with focused ion-beam milling," *Optics Express*, vol. 14, pp. 1505-1511, 2006.
- <sup>6</sup> I. Avrutsky, K. Chaganti, I. Salakhutdinov, and G. Auner, "Concept of miniature optical spectrometer using integrated optical and microoptical components," *Applied Optics*, 2006 (accepted).
- <sup>7</sup> I. Avrutsky, K. Chaganti, I. Salakhutdinov, and G. Auner, "Optical Micro-Spectrometer with Sub-Nanometer Resolution," *NSTI Nanotech*, p. Paper TU 21.02., May 7-11 2006.
- <sup>8</sup> J. Xu, G. Hu, G. Auner, and H. Ying, "Mass sensitivity of dual mode SAW delay lines on an AlN/sapphire structure," *Electron. Lett.*, vol. 41, p. 1254, 2005 2005.